

Lawrence Berkeley National Laboratory

Lawrence Berkeley National Laboratory

Title

Classification of Multiple Types of Organic Carbon Composition in Atmospheric Particles by Scanning Transmission X-Ray Microscopy Analysis

Permalink

<https://escholarship.org/uc/item/1fs7m8dn>

Author

Takahama, S.

Publication Date

2008-08-05

Peer reviewed

Classification of Multiple Types of Organic Carbon Composition in Atmospheric Particles by Scanning Transmission X-Ray Microscopy Analysis

S. Takahama^a S. Gilardoni^a L.M. Russell^{a,*} A.L.D. Kilcoyne^b

^a*Scripps Institution of Oceanography, University of California San Diego, 9500 Gilman Dr., Dept. 0221, La Jolla, CA 92093, USA*

^b*Advanced Light Source, Lawrence Berkeley National Laboratory, Berkeley, CA 94720, USA*

1 Abstract

2 A Scanning Transmission X-Ray Microscope at the Lawrence Berkeley National
3 Laboratory is used to measure organic functional group abundance and morphol-
4 ogy of atmospheric aerosols. We present a summary of spectra, sizes, and shapes
5 observed in 595 particles that were collected and analyzed between 2000 and 2006.
6 These particles ranged between 0.1 and 12 μm and represent aerosols found in a
7 large range of geographical areas, altitudes, and times. They include samples from
8 seven different field campaigns: PELTI, ACE-ASIA, DYCOMS II, Princeton, MI-
9 LAGRO (urban), MILAGRO (C-130), and INTEX-B. At least fourteen different
10 classes of organic particles show different types of spectroscopic signatures. Differ-
11 ent particle types are found within the same region while the same particle types
12 are also found in different geographical domains. Particles chemically resembling
13 black carbon, humic-like aerosols, pine ulitisol, and secondary or processed aerosol
14 have been identified from functional group abundance and comparison of spectra
15 with those published in the literature.

16 *Key words:* Aerosol, microscopy, Carbonaceous aerosol, organic, functional group,

18 **1 Introduction**

19 Atmospheric particles comprise sulfate, ammonium, nitrate, elemental carbon,
20 organic compounds, trace metals, crustal elements, and water (Seinfeld and
21 Pandis, 2006); organic material can account for 30-90% of the particle mass
22 (Lim and Turpin, 2002) and yet the relevant properties of the organic frac-
23 tion are not well characterized (Kanakidou et al., 2005; Fuzzi et al., 2006).
24 To address this knowledge gap, mass spectrometry, spectroscopy, and chro-
25 matography techniques are often employed to measure bulk and single-particle
26 chemical properties of ambient organic aerosols.

27 Hamilton et al. (2004) identified 10,000 chemical compounds in organic aerosol
28 sampled in an urban environment using direct thermal desorption coupled to
29 comprehensive gas chromatography-time of flight mass spectrometry (GCXGC-
30 TOF/MS). This quantity of information is difficult to use for interpretation
31 of atmospheric measurements and intractable for regional and global mod-
32 eling. Data clustering and classification provides a means by which we can
33 lump molecules or types of particles into characteristically similar groups,
34 reducing the complexity of subsequent analyses. Zhang et al. (2005a) de-
35 veloped a sequential multivariate regression method for application to Aero-
36 dyne Aerosol Mass Spectrometer (AMS)-measured mass fragments of the size-

* Corresponding Author. Address: Scripps Institution of Oceanography, University
of California San Diego, 9500 Gilman Dr., Dept. 0221, La Jolla, CA 92093, USA
Email address: lmrussell@ucsd.edu (L.M. Russell).

37 resolved bulk organic fraction of particles to derive the contributions from two
38 types: hydrocarbon-like and oxygenated organic aerosols (HOA and OOA, re-
39 spectively). This technique has been applied to the analysis of field measure-
40 ments in urban areas to show that these two types of compounds constitute
41 most of the organic aerosol (Zhang et al., 2005b; Kondo et al., 2007). Single-
42 particle mass spectrometry techniques have been able to use different cluster-
43 ing algorithms to provide information about the size and mixing states of in-
44 organic and organic components of aerosols based on elemental and molecular
45 fragment composition (Rhoads et al., 2003; Phares et al., 2003; Tolocka et al.,
46 2005; Bein et al., 2005), but often the mass fragments of carbon-containing
47 aerosols remain unresolved.

48 Particle morphology is also necessary for a complete understanding of how
49 these organic compounds affect the way they acquire mass from the gas phase
50 or interact with solar radiation (Kanakidou et al., 2005). For instance, shape
51 affects surface area for reactions that control rates of photochemical aging
52 (van Poppel et al., 2005) and direct radiative forcing by which particles scat-
53 ter and absorb sunlight. Heterogeneities can affect predictions of many at-
54 mospheric processes, including bulk chemical kinetics, surface reactions, mass
55 transport, thermodynamic partitioning, and phase transitions (Seinfeld and
56 Pandis, 2006).

57 For investigation of single particle morphology and composition, particle imag-
58 ing techniques such as Transmission Electron Microscopy (TEM), Environ-
59 mental Scanning Transmission Electron Microscopy (ETEM), Scanning Elec-
60 tron Microscopy (SEM), and Environmental Scanning Electron Microscopy
61 (ESEM) coupled with Electron Energy-Loss Spectroscopy (EELS) or Energy-
62 Dispersive X-Ray Spectrometry (EDX) can correlate shape and chemistry

63 (e.g., Hand et al., 2005; Johnson et al., 2005; Laskin et al., 2005, 2006), and
64 additional properties such as hygroscopicity (Semeniuk et al., 2006). These
65 electron microscopy techniques provide high spatial resolution, but the com-
66plementary spectroscopy methods provide limited information on chemical
67 composition or risk inducing radiation damage in the sample (Warwick et al.,
68 1997; Braun et al., 2005a).

69 Fuzzi et al. (2006) suggest possible organic aerosol classification categories
70 based on source, and techniques by which the organic aerosol fraction can
71 be used to map measurements to the suggested source categories. Near Edge
72 X-Ray Absorption Fine Structure (NEXAFS) spectrometry uses synchrotron-
73 generated soft X-ray beams which provide the energy resolution necessary to
74 distinguish organic functional groups absorbing at different bonding energies of
75 carbon-containing molecules (e.g., Stöhr, 1992; Russell et al., 2002; Myneni,
76 2002; Maria et al., 2004; Braun, 2005). Samples are analyzed under atmo-
77 spheric pressure, resulting in reduced loss of semi-volatile material commonly
78 found in organic constituents of aerosols. We use this spectrometry method
79 with a Scanning Transmission X-Ray Microscope (STXM) for analysis of our
80 samples.

81 In microscopy analysis, discretion is warranted in using size and shape infor-
82 mation for data clustering and also for general interpretation of the results, as
83 spherical particles can be elongated or smeared against the substrate (Barkay
84 et al., 2005), and loosely-bound constituents of a particle may be disaggre-
85 gated in the process of sample collection via impaction. Therefore, chemical
86 properties are considered as the primary means of classification in this work.

87 Russell et al. (2002) and Maria et al. (2004) reported STXM analysis of par-

88 ticles collected from several different regions representing different types of
89 aerosols: Eastern US combustion aerosol from Princeton, NJ, African mineral
90 dust over the Caribbean Sea (PELTI campaign), Asian combustion aerosol over
91 the Sea of Japan (ACE-ASIA campaign). In this study, we combine these par-
92 ticles with a meta-analysis of additional particles collected during DYCOMS
93 II, MILAGRO, and INTEX B, providing several categories for chemical prop-
94 erties and morphologies observed in ambient particles, thereby relating them
95 to the location and period during which they were collected.

96 **2 Methods**

97 *2.1 Geospatial domain*

98 Samples analyzed in this paper were collected during the Passing Efficiency
99 Low Turbulence Inlet experiment (PELTI), a campaign to characterize aerosol
100 in the Caribbean (Huebert et al., 2004); Aerosol Characterization Experiment
101 (ACE-Asia), a campaign to study aerosol in China, Japan, and Korea (Huebert
102 et al., 2003) during April 2001; Second Dynamics and Chemistry of Marine
103 Stratocumulus field study (DYCOMS II), a study of marine stratocumulous
104 clouds conducted during July 2001 southwest of San Diego, CA, USA (Stevens
105 et al., 2003); Megacity Initiative: Local and Global Research Observations
106 (MILAGRO), a mega-city characterization campaign involving measurement
107 at an urban site (MCMA) and aloft via aircraft (MIRAGE C-130) during
108 March 2006 (<http://www.eol.ucar.edu/projects/milagro/>); and INTEX-B, a
109 campaign to measure Asian pollution outflow along the Pacific Northwest
110 coast of the US in May 2006 (<http://www.espo.nasa.gov/intex-b/>). Samples

111 collected at a ground site in Princeton, NJ, USA, in August 2003 (Maria et al.,
112 2004) are also included in this analysis.

113 *2.2 Sample collection and analysis*

114 Particles were collected on silicon nitride windows (Si_3N_4 ; Silson Ltd.) mounted
115 on a rotating impactor (Streaker; PIXE International, Inc.) for all samples ex-
116 cept those samples in Princeton, NJ. For these samples, lacey-carbon TEM
117 grids were used as the substrate. For both aircraft and ground site measure-
118 ments, aluminum or copper tubing was used to draw air into the impactor
119 at 1 Lpm. Sampled grids and windows were analyzed at the Advanced Light
120 Source at Lawrence Berkeley National Laboratories (Berkeley, CA) Beamlines
121 5.3.2, 7.0.1, and 11.0.2 in a He-filled chamber maintained at 1 atm. Transmis-
122 sion of photons at energy levels between 278 and 305 eV were measured over
123 a minimum spatial resolution of 30 nm and converted to optical density, using
124 a protocol described by Russell et al. (2002) and Maria et al. (2004).

125 *2.3 Spectral classification and analysis*

126 Spectra were classified according to the presence of functional groups iden-
127 tified by Russell et al. (2002). Alkyl, ketonic carbonyl, carboxylic carbonyl,
128 and alkene (or aromatic) groups are abbreviated as $\text{R}(\text{CH}_n)\text{R}'$, $\text{R}(\text{C}=\text{O})\text{R}$,
129 $\text{R}(\text{C}=\text{O})\text{OH}$ and $\text{R}(\text{C}=\text{C})\text{R}'$, respectively. R represents any alkyl chain, R'
130 represents H or any alkyl chain, and $n=0, 1, \text{ or } 2$ (Russell et al., 2002). π^* -
131 bonds for molecules containing these functional groups absorb near $285\pm 0.2\text{eV}$
132 ($\text{R}(\text{C}=\text{C})\text{R}'$), 286.7 ± 0.2 ($\text{R}(\text{C}=\text{O})\text{R}$), 287.7 ± 0.7 ($\text{R}(\text{CH}_n)\text{R}'$), and 288.7 ± 0.3

133 eV (R(C=O)OH). Additionally, carbonate (CO_3^{2-}) absorbs around 290.4 ± 0.2
134 eV and potassium (K) $L_{2,3}$ edges at 297.4 ± 0.2 and 299.9 ± 0.2 eV (Russell et al.,
135 2002; Yoon et al., 2006). Images were aligned using the Zimba subroutine im-
136 plemented in aXis2000 (<http://unicorn.mcmaster.ca/aXis2000.html>); energy
137 levels were aligned a posteriori to account for shifts in spectra energies. Spec-
138 tra were adjusted for background absorbance ($278 < \text{eV} < 283$) and normalized
139 to total carbon content ($301 < \text{eV} < 305$) (Maria et al., 2004).

140 Spectra were classified using their full dimensionality (i.e. absorbance at en-
141 ergy levels scanned and interpolated over a grid consisting of 82 points be-
142 tween 280 and 305 eV), which can be more selective than classification based
143 on pre-selected peak abundance. First, k -means and hierarchical clustering
144 algorithms were applied on a data set after having removed 5 percent of the
145 most extreme spectra as determined by Euclidean distance from the grand
146 spectra average (thus reducing the possibility of creating classes that contain
147 single samples). After application of these algorithms, group centers were used
148 as a training set for k -nn to assign memberships for all spectra. Unsupervised
149 classification algorithms excel at single-objective optimization, i.e. finding a
150 solution which minimizes the sum-of-squares between spectra and cluster cen-
151 ters for all spectra. However, we qualitatively considered additional criteria for
152 classification, such as our understanding of chemical similarity as determined
153 by interpretation of the spectra, sampling conditions, times, and locations,
154 and this information was incorporated through manual redistribution of spec-
155 tra grouped by the quantitative algorithms. The final procedure increases the
156 overall sum and variance of sum-of-squares from cluster centers, but effectively
157 allows construction of a few groups with small within-cluster sum-of-square
158 values that are believed to have atmospherically relevant similarities.

159 For semi-quantitative characterization of particle classes, deconvolution of the
160 spectra was performed according to a method similar to that described by
161 Lehmann et al. (2005) and Hopkins et al. (2007). Gaussian peaks with FWHM
162 constrained to 0.5-2 eV were fitted at each of the peak locations described
163 above and also at 289.7 eV, and two broader peaks to represent σ^* -transitions
164 at 294 and 303 eV constrained to 0.5-6 and 0.5-8 eV, respectively. The ion-
165 ization threshold was approximated with an arctangent function with 1 eV
166 FWHM.

167 For classes of spectra believed to contain black carbon, %sp² hybridization
168 was calculated (Hopkins et al., 2007) to characterize the graphitic nature of
169 the particle. This value is calculated according to the equation,

$$170 \quad \%sp^2 = \left(\frac{A_{R(C=C)R'}^{(sample)}}{A_{Total}^{(sample)}} \times \frac{A_{Total}^{(HOPG)}}{A_{R(C=C)R'}^{(HOPG)}} \right) \cdot 100\%.$$

171 While Hopkins et al. (2007) used energies between 280 and 320 eV to calculate
172 A_{Total} , we use energies between 280 and 305 eV because of data availability. Be-
173 cause the energy range used in normalization is consistent for both the samples
174 and the reference HOPG spectra, the difference between our reported results
175 and those of (Hopkins et al., 2007) is expected to be small.

176 *2.4 Morphology classification*

177 Particles can be found in many different types of shapes: single sphere, single
178 irregular solid (e.g., crystal), and aggregate of many particles. For this analy-
179 sis, the particles were classified visually as spherical or irregular based on the
180 285 eV STXM image of their impacted shape. Geometric sizes were calculated
181 by averaging physical measurements along perpendicular axes of the particle.

182 Heterogeneities can include agglomerations of a single phase of different chem-
183 ical compositions or co-existence of multiple phases, which can occur in many
184 different configurations (Seinfeld and Pandis, 2006). Although an exhaustive
185 analysis of heterogeneities is beyond the scope of this work, the heterogeneities
186 were characterized for which the spectral differences of different regions of a
187 single particle were significant.

188 *2.5 Backtrajectory analysis*

189 The National Oceanic and Atmospheric Administration Hybrid Single-Particle
190 Lagrangian Integrated Trajectory (HYSPLIT, Draxler and Rolph, 2003; Rolph,
191 2003) model was used to calculate backtrajectories for a few scenarios. For
192 these calculations, the FNL meteorological data were used as inputs. Follow-
193 ing the recommendations of Gebhart et al. (2005), the trajectories were run
194 in an ensemble mode to allow the model to effectively simulate over a range
195 of initial starting locations and heights. A horizontal grid offset of 0.3 and
196 a vertical offset of 0.1 sigma coordinates were specified for the simulation.
197 According to the resolution of the FNL input data set, this corresponds to
198 approximately 30 km horizontal and 90-120 m vertical displacement over 27
199 simulations for each ensemble.

200 *2.6 Simultaneous filter measurements*

201 During all field sampling campaigns in which samples for STXM analysis were
202 collected, particles were concurrently collected on a collocated Teflon-filter
203 sampler. These filters were analyzed by FTIR for organic functional groups

204 (Maria et al., 2003, 2004). Some of these filters were analyzed by X-ray fluo-
205 rescence (XRF) by Chester LabNet (Tigard, OG) for elemental composition
206 to aid in source identification.

207 **3 Results and Discussion**

208 Table 1 summarizes the particles included in our classification scheme. A total
209 of 595 particles collected between 2000 and 2006 were analyzed. Altitudes of
210 samples ranged between 30 and 4400 m. Of these particles, 244 were classified
211 as being spherical; 54 contained heterogeneities. More than one spectrum may
212 be associated with a single particle if its chemical heterogeneities are resolv-
213 able; this resulted in 680 different spectra. One-hundred and forty-two of these
214 spectra were not interpretable either because the signal was either saturated
215 or lost in the noise. The geometric diameters of particles analyzed spanned
216 from 0.1 μm to 12 μm , with 364 particles below one micron. Over 80% of
217 the 595 particles exhibited statistically significant spectral intensities below
218 283 eV, indicating that the majority of these organic particles were internally
219 mixed with non-carbonaceous material (Maria et al., 2004; Lehmann et al.,
220 2005).

221 Fourteen categories are used to classify all of the 595 resolved particles based
222 on similar spectral features. Between one and 76 particles were analyzed on
223 each of the 38 slides; the number of spectra categories on each slide ranged
224 from one to nine. Figure 1 shows the different spectra types and Figure 2 shows
225 the corresponding size, shape classification, and project from which each spec-
226 tra was collected. Figure 3 presents example images of particles corresponding
227 to each particle type. These images are not meant to be representative of each

228 category, but, collectively, illustrates some of the diversity observed in mor-
229 phology of ambient particles. While there is insufficient evidence to assert this
230 set of categories is a complete representation of atmospheric organic particle
231 types, it is surprising that a few types appear in many disparate regions of the
232 atmosphere. Other particle types appear only in one or two specific regions,
233 suggesting their sources may be more limited.

234 3.1 Spectra types and descriptions

235 The most ubiquitous type of spectra was that dominated by an $\text{R}(\text{C}=\text{O})\text{OH}$
236 peak (Figure 1a), designated as type a. There were 136 particles that exhibited
237 this spectrum. These types of particles were found at some of the samples from
238 every project and over a wide size range, in both spherical and irregular form.
239 A particularly high number of submicron, spherical particles of this type were
240 found in DYCOMS II and ACE-Asia.

241 Type b spectra (Figures 1b,2b) were observed exclusively on a single sam-
242 ple from Research Flight 6 during the MILAGRO campaign. These spectra
243 strongly indicated the presence of both $\text{R}(\text{C}=\text{C})\text{R}'$ and $\text{R}(\text{C}=\text{O})\text{OH}$ bonds
244 (Figure 1b). All type b particles (21) were submicron and spherical (no hetero-
245 geneities were detected). Particles on this slide were collected on the afternoon
246 of a holiday weekend (18 March 2006) northeast of Mexico City. Absorbances
247 in $\text{R}(\text{C}=\text{C})\text{R}'$ and $\text{R}(\text{C}=\text{O})\text{OH}$ of type b spectra are distinguished by very
248 strong and distinct peaks.

249 Type c (Figures 1c,2c) was predominantly found in the ACE-Asia particles,
250 and shows a peak in the $\text{R}(\text{C}=\text{O})\text{R}$ region in addition to $\text{R}(\text{C}=\text{O})\text{OH}$ and

251 R(C=C)R'. These particles were identified as being surface-oxidized primary
252 carbon, possibly black carbon (Maria et al., 2004). There were 25 type c
253 spectra, only one of which was from the INTEX-B study. Type c included
254 spherical and irregular particles. The spherical ones ranged from 0.3 to 1.4 μm
255 in diameter ($n = 15$), and irregular ones ranged from 0.6 to 5 μm in diameter
256 ($n = 10$). These particles were generally not associated with heterogeneities.

257 Type d (Figures 1d,2d) was observed in almost every field campaign, espe-
258 cially in airborne measurements. Type d spectra are dominated by a strong
259 absorbance in the R(C=C)R' region (Figure 1d), without the distinct peaks
260 observed in Figure 1b. These particles are generally submicron and irregular,
261 with a few exceptions. While many of the type d particles were irregular, only
262 one of them had a detectable heterogeneity.

263 Figure 1e shows type e spectra with strong absorbance around R(C-H)R' and
264 R(C=O)OH in addition to R(C=C)R'. These particles were collected mostly
265 on the aircraft during MILAGRO and also in Princeton, NJ.

266 Type f (Figures 1f,2f) was found exclusively in PELTI samples, showing a
267 strong R(C=O)OH abundance and high absorbances in the K region, consis-
268 tent with either a dust or biomass burning source. Concurrent absorbance in
269 the region of CO_3^{2-} absorbance suggests a strong mineral contribution.

270 Figure 1g shows spectra of particles collected mostly in Princeton for combustion-
271 related aerosols (Maria et al., 2004). Additional type g samples were also found
272 in MILAGRO aircraft measurements. These show a strong absorbance in the
273 R(C=C)R' region and amorphous absorbance in R(C-H)R' and R(C=O)OH
274 just before the carbon K-edge.

275 Type h spectra shown in Figures 1h,2h were collected mostly in Mexico City
276 with the exception of one collected on board the NCAR C-130 near Mexico
277 City - these particles are spherical and supermicron. Because of their size, these
278 particles are often associated with heterogeneities, in the form of inorganic
279 inclusions or enrichment of $R(C=O)OH$ at the surface.

280 Five additional spectra types include spectra with a common presence of
281 functional groups but with varying abundances of each component (Figures
282 1 and 2, i-m). Spectra in Figure 1i show strong absorbance in regions of
283 $R(C=O)OH$ and $R(C=C)R'$. Type j spectra are similar to type c spectra
284 (ACE-Asia particles) with $R(C=C)R'$, $R(C=O)R$, $R(C=O)OH$ absorbance
285 but weaker $R(C=C)R'$. Type k spectra show the carbon K-edge but no signif-
286 icant peaks. Type l shows $R(C=C)R'$ absorbance, although $R(C=O)OH$ is not
287 discernible. Type m shows absorbance in $R(C=C)R'$ and $R(C=O)R$, but in
288 general $R(C=O)OH$ absorbance is not apparent. Altogether, these five groups
289 account for 35% of the particles.

290 Type n shows a maximum peak between $R(C=H)R'$ and $R(C=O)OH$ ab-
291 sorbance regions with additional unidentified peaks (Figure 1n). Such shifts
292 in peak absorbance energies can occur in response to subtle differences in lo-
293 cal coordination environment. These particles were collected mostly in Mexico
294 City but also aloft during MILAGRO and INTTEX-B, and these particles were
295 generally found to be larger than $1 \mu m$ (Figure 2n).

296 3.2 Atmospheric implications

297 The measured properties of organic functional groups in atmospheric particles
298 and comparison of overall absorbance features with reference spectra suggest
299 possible particle sources and radiative impacts. Below we consider the poten-
300 tial atmospheric sources of some of the mixture types we have identified, by
301 classifying them as combustion-derived, carboxylic-acid dominated, biogenic
302 aerosols, and unidentified.

303 3.2.1 Strongly aromatic aerosols

304 Types b, c, d, e, g, h, and m share significant absorbance in the R(C=C)R'
305 region (Figure 5A) and possibly indicate the presence of sp²-bonding of car-
306 bon found in soot or black carbon, suggesting that these particles will most
307 likely be strongly absorbing. The degree of graphitization is dependent on fuel
308 type and conditions of combustion (Andreae and Gelencser, 2006; Bond and
309 Bergstrom, 2006), which Braun and coworkers have observed by NEXAFS and
310 x-ray scattering in controlled studies (Braun, 2005; Braun et al., 2005b, 2006a;
311 di Stasio and Braun, 2006; Braun et al., 2007). Hopkins et al. (2007) used an
312 %sp² hybridization metric to distinguish among different types of spectra mea-
313 sured for reference and field samples of aerosol, and these values ranged from
314 29-82%. In our particle classes, we observed mean values ranging from 28-72%
315 (Table 2). Significant differences in %sp² within each particle class exists such
316 that relating variations in NEXAFS spectra of ambient particles to combus-
317 tion conditions is difficult, but it is sufficient to note that sp²-hybridization in
318 graphitic carbon is strongly related to photoabsorption and index of refraction
319 (Bond and Bergstrom, 2006).

320 While “black carbon” is often used synonymously with “soot” to refer to the
321 major light-absorbing component of aerosols, Andreae and Gelencser (2006)
322 note that the contribution in light absorption from other carbonaceous com-
323 pounds can also be significant. “Brown carbon” compounds may include other
324 anthropogenic combustion-related compounds such as coal tar or products of
325 organic matter (e.g., lignin) pyrolysis, but also biogenic materials such as hu-
326 mic or fulvic substances, humic-like substances (HULIS), products of aromatic
327 hydroxy acid oxidation and reactions of organic compounds in sulfuric acid
328 particles (Andreae and Gelencser, 2006).

329 Backtrajectories of type c and d particles were analyzed by Maria et al. (2004)
330 and suggest their origins may lie in combustion sources. Several possible ori-
331 gins of type b spectra were considered, including contamination. Another
332 compound which has a strong signature of absorbance in $R(C=C)R'$ and
333 $R(C=O)H$ is phthalic acid (Plaschke et al., 2004), commonly used as plas-
334 ticizer in many plastic materials (and possibly a contributor to sampling ar-
335 tifact; Fraser et al., 2003; Ray and McDow, 2005). Out of the 30 particles
336 identified on this slide, 9 of the particles did not contain this chemical finger-
337 print, though such evidence may be produced by preferential absorption by
338 a certain class of particle. The lack of this type of spectra in other samples,
339 however, indicates that if it were contamination, it would be generated from
340 an isolated event. So other explanations are more likely. For instance, phthalic
341 acid is often found in atmospheric aerosols (e.g., Limbeck et al., 2001; Rudolph
342 and Stupak, 2002; Ray and McDow, 2005; Kawamura and Yasui, 2005), from
343 direct emission by combustion sources (Kawamura and Kaplan, 1987) or sec-
344 ondary formation by oxidation of aromatic hydrocarbons (Jang and McDow,
345 1997; Fraser et al., 2003; Fine et al., 2004; Wang et al., 2006). However, type

346 b spectra may be considered only partially phthalic-acid-like, in that the pro-
347 portion of the peaks are reversed. For type b particles the relative abundance
348 of $R(C=O)H$ is greater than that of $R(C=C)R'$, while the opposite is true in
349 phthalic acid. It is also possible that type b spectra represent another class of
350 compounds with strong sp^2 -bonding combined with carboxylic acid groups.

351 Backtrajectories for type b particles (Figure 4A) indicate that they traveled
352 from the southeast of Mexico City at least 1,500 m above ground level. Con-
353 current measurements of elemental composition by XRF indicate relatively
354 high loadings of Barium. Barium is also used in rubber production and can
355 be a airborne product of tire abrasion (e.g., Weckwerth, 2001; Varrica et al.,
356 2003), but such particles are often coarse and irregularly-shaped - unlike type
357 b particles (Figure 3b). Barium can also be found in pyrotechnic aerosols (i.e.
358 from fireworks; Liu et al., 1997). The day on which this sample was collected
359 was a holiday weekend in Mexico. Magnesium is often associated with Barium
360 in pyrotechnic particles, but XRF measurements indicate negligible concentra-
361 tions were present in this sample. Since the relative quantities of Barium and
362 Magnesium in these types of aerosols can vary (Liu et al., 1997), the absence
363 may be a result of the detection limit.

364 Another possible source of Barium is volcanic emissions. The backtrajectory
365 analysis indicates the air parcel passed by the location of Popocatepetl, an
366 active volcano that contributes to the SO_2 burdens in the nearby City. It is
367 possible that type b particles are derived from this source. The XRF analysis
368 also indicates high loadings of Sulfur, which is in agreement with the findings
369 by Obenholzner et al. (2003), who measured Ba-S-O particles (presumably
370 found in the form of barite, $BaSO_4$) from this volcanic plume.

371 The other types of particles in this category were prevalent over many loca-
372 tions and field campaigns indicating non-unique origins. However, comparisons
373 with reference spectra of soot particles examined under various conditions
374 (e.g., Brandes et al., 2004; Braun et al., 2004, 2005a,b; Michelsen et al., 2006;
375 Lehmann et al., 2005; some examples shown with average spectra from 1 in
376 Figures 6A and 6B) show many similarities, including the absorption of X-
377 rays in $R(C=C)R'$ and $R(C=O)OH$ regions. Differences may arise from one of
378 many possible reasons. For instance, soot spectra can vary depending on fuel
379 source and engine loading (Braun et al., 2005a,b), condensed-phase hydrocar-
380 bons can be co-emitted with soot as a coating layer (Braun et al., 2004; Kis
381 et al., 2006), and rapid internal mixing with inorganic compounds have been
382 observed in freshly emitted soot particles in an urban environment (Johnson
383 et al., 2005). In the absence of these mixing mechanisms, however, the hy-
384 drophobicity of soot and its low probability for removal by wet deposition
385 (Lim et al., 2003) may account for the frequent observation of these particles,
386 especially at high altitudes.

387 Mishchenko and coworkers found that the single scattering albedo calculated
388 by Mie theory is not very sensitive to non-sphericity (Mishchenko et al., 1995),
389 but shape considerations can still influence the radiative budget if the excess
390 surface area of irregular particles over that of spherical particles is taken into
391 account. Scattering is a strong function of hygroscopic growth of particles.
392 Irregular particles of initially hydrophobic composition such as soot can be-
393 come more hydrophilic with increasing surface area (van Poppel et al., 2005;
394 Petters et al., 2006). Of our soot-like particles, 70 out of 88 are irregular. Our
395 sample collection method may bias our results toward an irregular classifi-
396 cation as the process of impaction can alter the shape of spherical particles.

397 Spherical particles may indicate that these hydrophilic conversions have taken
398 place and these soot inclusions have water associated with them (wet particles
399 are almost always spherical, Seinfeld and Pandis, 2006). While the resolution
400 of STXM does not permit rigorous fractal analysis, van Poppel et al. (2005)
401 found that when the fractal properties of fresh soot aggregates are explicitly
402 calculated with 3D images assembled from TEM and electron tomography,
403 the surface area increased by an order of magnitude over that of a spherical
404 particle of “equivalent” size. Taking into account only the (sulfuric acid) con-
405 densation pathway, their simulations in a global climate model suggested that
406 BC lifetime and direct radiative forcing are currently underestimated by 40%.
407 The coating will further accelerate the black-carbon absorption enhancement
408 described by Jacobson (2000).

409 Mishchenko et al. (2004) found that agglomerations of scattering aerosol com-
410 ponents that retain chemically distinct phases have similar optical properties
411 to an ensemble of externally mixed particle population composed of the same
412 species. However, black carbon internally mixed (coated) with even purely
413 scattering chemical components can become more absorbing and contribute
414 significantly to climate change (Jacobson, 2000). NEXAFS spectra are sensi-
415 tive to combustion conditions under which organic aerosols are formed and to
416 subsequent atmospheric processing by ultraviolet radiation and oxidants, pro-
417 viding complementary information for source identification of particles (Braun,
418 2005; Braun et al., 2006a; di Stasio and Braun, 2006; Braun et al., 2007). Sev-
419 eral authors (e.g., Posfai et al., 1999; Johnson et al., 2005) report that soot
420 coated by inorganics is common in the atmosphere. In our data, 82 out of
421 88 soot-like particles contain non-zero intensities below 283 eV, showing the
422 presence of non-carbonaceous components in the particles.

423 3.2.2 Multiple-transition aerosols

424 Types i and j include particles that show absorptions in $R(C=C)R'$ (though
425 relatively weaker than the soot-type particles), $R(C=O)R$, $R(C-H)R'$ and
426 $R(C=O)OH$ (Figure 5B); some studies identify absorbances around 286 eV
427 as those belonging not only to ketonic carbonyl but also to C-OH resonances
428 of hydroxylated aromatics such as phenols (e.g., (Lehmann et al., 2005; Schu-
429 macher et al., 2005; Braun, 2005)), which can be significant for products of
430 wood burning (Braun, 2005). These particle types share spectral features most
431 similar to those found in biogenic sources: humic and fulvic acids (Ade and
432 Urquhart, 2002), soil substances (Solomon et al., 2005; Lehmann et al., 2005;
433 Schumacher et al., 2005), and biomass combustion (Braun, 2005; Tivanski
434 et al., 2007). Reference spectra for some of these aerosols published in the
435 literature are shown with average spectra of type i and j particles in Figures
436 6C and D.

437 %sp² hybridization in biomass burning aerosols studied by Hopkins et al.
438 (2007) ranged from 5-41 %; Suwannee river humic and fulvic acids studied
439 by the same authors were 28 and 29%, respectively, indicating generally lower
440 values than those calculated for black carbon aerosols. The average %sp² hy-
441 bridization calculated for i and j particles (18 and 30%, respectively) are in
442 qualitative agreement with this trend. For particles generated from biomass
443 (wood) combustion, however, it is possible that the absorbance at 285 eV can
444 be attributed to polycyclic aromatic hydrocarbons (PAHs; Rogge et al., 1998)
445 rather than the sp²-bonding anticipated in black carbon.

446 Humic-like substances (HULIS) in the atmosphere have received considerable
447 attention in the aerosol literature (e.g., Gelencser et al., 2002; Gysel et al.,

448 2004; Hoffer et al., 2006; Graber and Rudich, 2006 and references therein).
449 In comparison with reference spectra of humic and fulvic acids studied by
450 Ade and Urquhart (2002), particles contained in types i and j categories may
451 be examples of atmospheric particles identified elsewhere as HULIS. Tivanski
452 et al. (2007) studied tarballs, a special class of aerosols generated by biomass-
453 burning events, also by NEXAFS spectroscopy, and observed similarities in
454 the presence of $R(C=C)R'$, $R(C=O)R$, and $R(C=O)OH$ transitions as seen in
455 similar reference acid standards.

456 HULIS in aerosols have polycyclic ring structures and hydrocarbon side chains,
457 hydroxyl, carboxyl, and carbonyl groups (Graber and Rudich, 2006), and this
458 is in agreement with our observation of X-ray absorbances over a wide range
459 of energies. Despite the overall resemblance to humic and fulvic acid samples,
460 there are a few important spectral differences. The differences may reflect the
461 dissimilarity between atmospheric HULIS and fulvic acids and laboratory-
462 generated macromolecules, most importantly in the small molecular size of
463 the former type (Graber and Rudich, 2006). Graber and Rudich (2006) at-
464 tribute this difference to a number of possible causes, including abiotic for-
465 mation mechanisms in airborne particles, processing (i.e. photo-oxidation) in
466 the atmosphere, and ionic interference toward the congregation of polymeric
467 units.

468 If type i and j particles are indeed derived from sources of brown carbon
469 substances described by Andreae and Gelencser (2006), they may serve as ad-
470 ditional light-absorbing material in the atmosphere. For instance, the water-
471 soluble HULIS obtained from biomass burning aerosol was shown to absorb
472 strongly at shorter wavelengths, to the sum of about 7% over the solar spec-
473 trum (Hoffer et al., 2006). Water-soluble material resembling humic substances

474 has been observed to have low to comparable water uptake to secondary organic
475 aerosol (SOA) and may alter the water uptake and phase-transition properties
476 of inorganic aerosol (Gysel et al., 2004; Badger et al., 2006). Of 115 of these
477 types of particles, 70 were spherical.

478 3.2.3 Carbonate and carboxylic-carbonyl aerosol

479 Type f particles were collected over the Caribbean Ocean during the PELTI
480 campaign (Maria et al., 2002). As seen in Figure 5C, these particles show
481 high relative abundance of $R(C=O)H$ and also CO_3^{2-} . Type f spectra strongly
482 resemble the spectrum of pine Ultisol soil collected in Puerto Rico (Ade and
483 Urquhart, 2002, shown in Figure 6C and D). These particles may have either
484 traveled from Africa with dust of similar composition as indicated by the
485 backtrajectory analysis (Figure 4B), or they could be produced from local
486 sources by vertical mixing of soil dust particles.

487 3.2.4 Carboxylic-carbonyl dominated organic aerosol

488 Type a particles have a strong carboxylic carbonyl signature (Figure 5D),
489 and these particles are likely to behave differently from the light-absorbing
490 carbon in the atmosphere. Carboxylic acids and oxygenated compounds are
491 relatively soluble and can thus be significant players in direct radiative forcing
492 and also as cloud condensation nuclei (Kanakidou et al., 2005). Myhre and
493 Nielsen (2004) calculated that several binary mixtures of organic acids (oxalic,
494 malonic, tartronic, succinic, and glutaric) with water have a purely scattering
495 effect, which is less dependent on component than on mass mixing ratio in
496 solution. Fifty-eight of 136 type a particles were spherical. For hydrophilic

497 species to be irregular suggests that impaction resulted in an asymmetrical
498 distortion of particle shape, or in efflorescence of the particle. Carboxylic acids
499 are the dominant product of reactions yielding SOA (Yu et al., 1999; Glasius
500 et al., 2000), contributing as much as 30% to the SOA mass yield of α -pinene
501 ozonolysis (Yu et al., 1999). Their formation mechanism suggests one reason
502 for their ubiquity in different locations and field sampling campaigns.

503 *3.2.5 Unidentified spectra types*

504 The remaining spectra types have not been identified with specific organic
505 compounds or sources, in part because of the paucity of reported spectra for
506 other potential sources of organic aerosol (e.g. isoprene, glyoxyl, secondary
507 organic aerosol, condensation products of primary emissions of intermediate
508 volatility). Furthermore, mixing of particle components and heterogeneous
509 reactions in the atmosphere will induce chemical transformations in the aerosol
510 phase, some or all of which will affect the measured NEXAFS spectra.

511 The main peak in type n is in the region of $R(C=O)OH$ but is shifted slightly
512 from similar peaks observed in all other samples, indicating a bonding envi-
513 ronment different from those found in the rest of the particles. The origin and
514 chemistry that drives this shift in absorbance energy level is unclear. Type
515 k and l particles lack distinct spectral features; in particular, there is an ab-
516 sence of a carboxylic peak. The total carbon to total mass ratio calculated by
517 the method of Maria et al. (2004) indicates that on average, the normalized
518 carbon content of these particles are comparable to those from other parti-
519 cles, suggesting that the absence of these peaks is not necessarily due to the
520 lack of carbonaceous material. Several alternative explanations are possible.

521 Braun and coworkers have studied the effect of chemical changes to diesel par-
522 ticulate matter and the impact on molecular bonding observed by NEXAFS.
523 In one study, Braun (2005) showed that diesel particulate matter “weath-
524 ered” in ambient humidity and sunlight for 10 days resulted in a decrease in
525 $R(C=O)OH$ and $C-OH$ resonances but an increase in $R(C=C)R'$. Braun et al.
526 (2006b) observed decomposition of carboxyl groups in alginic acid and diesel
527 soot extracts to carbonate by NEXAFS under intense X-Ray irradiation. The
528 authors of the study suggest such transformations are likely to be slow but
529 possible in soot particles in the atmosphere. In addition, carboxylic acids can
530 be converted into high-molecular weight organic compounds (Mochida et al.,
531 2006), or gas-phase oxidants can increase the oxygen content in the reacted
532 organic layer (Katrib et al., 2005) which might decrease the $R(C=O)OH$ ab-
533 sorbance and increase the $R(C=O)R'$ absorbance. The collective effects of all
534 aging processes on the chemical transformation of aerosols in the atmosphere
535 are still uncertain, and the extent that such chemical changes can be detected
536 with NEXAFS $C(1s)$ is not yet known.

537 4 Conclusions

538 As a first approximation, sampling an air mass with ~ 1000 particles/cm³ at
539 1 Lpm for 20 minutes will result on the order of 10^7 particles. Of the ones
540 that can be identified by STXM (> 100 nm), we typically analyze between
541 1 and 76 particles per sample. The frequency of occurrence of certain types
542 of spectra and morphology suggest that they may represent a significant part
543 of the ambient particle population, even though this small sample cannot be
544 extrapolated to all atmospheric particles.

545 Spectra were classified into 14 types on the basis of similarities in the presence
546 and relative abundance of organic functional groups. Compared to classifica-
547 tion techniques by other instruments (e.g., Aerosol Mass Spectrometer, Zhang
548 et al., 2005a; ETEM, Semeniuk et al., 2006), STXM provides more detailed
549 organic classification by chemical bond characteristics for individual parti-
550 cles using NEXAFS. Using this information, our work suggests one scheme
551 for representing the multitude of condensed-phase organic compounds in the
552 atmosphere with a reasonable number of mixtures and particle types.

553 The observed combinations of particle shape and carbon K-edge spectra indi-
554 cate that many classes of organic particles exist in the atmosphere, even within
555 the same geographical location. A few spectra classes were unique to specific
556 locations, but many types of carbonaceous particles with similar molecular
557 bonding structures exist in disparate regions around the globe, suggesting com-
558 mon types of sources and similar processes of atmospheric transformations for
559 organic particles. Examining similarities with reference spectra, black carbon,
560 humic-like, pine ultisol, and secondary or processed aerosols were identified in
561 several field campaigns in the northern hemisphere. The existence of different
562 types of organic compounds on different organic particles may affect CCN
563 properties, interaction with solar radiation, and aerosol chemistry differently.

564 **Acknowledgements.**

565 The authors acknowledge grant support for this work from DOE (W/GEC05-
566 010, MPC35TA-A5), NSF (ATM-0511772, ATM-0408501, ATM-0002035, ATM-
567 0104707), and the James S. McDonnell Foundation. In addition, valuable assis-
568 tance was provided in using and interpreting ALS facilities by S.C.B Myneni
569 and M.K. Gilles. J.R. Anderson, M.D. Rivera, R. Ramos, and the science

570 and operation teams of the field experiments PELTI, ACE-Asia, DYCOMS
571 II, MILAGRO, and INTEX-B also provided enormous assistance in sample
572 collection. The authors also thank the anonymous reviewers for their insight
573 and helpful comments.

574 **References**

575 Ade, H., Urquhart, S. G., 2002. Chemical Applications of Synchrotron Radia-
576 tion. World Scientific Publising, Singapore, Ch. NEXAFS Spectroscopy and
577 Microscopy of Natural and Synthetic Polymers.

578 Andreae, M. O., Gelencser, A., 2006. Black carbon or brown carbon? The
579 nature of light-absorbing carbonaceous aerosols. *Atmos. Chem. Phys.* 6,
580 3131–3148.

581 Badger, C. L., George, I., Griffiths, P. T., Braban, C. F., Cox, R. A., Abbatt,
582 J. P. D., 2006. Phase transitions and hygroscopic growth of aerosol particles
583 containing humic acid and mixtures of humic acid and ammonium sulphate.
584 *Atmos. Chem. Phys.* 6, 755–768.

585 Barkay, Z., Teller, A., Ganor, E., Levin, Z., Shapira, Y., 2005. Atomic force
586 and scanning electron microscopy of atmospheric particles. *Microsc. Res.*
587 *Tech.* 68 (2), 107–114.

588 Bein, K. J., Zhao, Y. J., Wexler, A. S., Johnston, M. V., 2005. Speciation of
589 size-resolved individual ultrafine particles in Pittsburgh, pennsylvania. *J.*
590 *Geophys. Res. - Atmos.* 110 (D7).

591 Bond, T. C., Bergstrom, R. W., 2006. Light absorption by carbonaceous par-
592 ticles: An investigative review. *Aerosol Sci. Technol.* 40 (1), 27–67.

593 Brandes, J. A., Lee, C., Wakeham, S., Peterson, M., Jacobsen, C., Wirick,
594 S., Cody, G., 2004. Examining marine particulate organic matter at sub-

595 micron scales using scanning transmission X-ray microscopy and carbon
596 X-ray absorption near edge structure spectroscopy. *Mar. Chem.* 92 (1-4),
597 107–121.

598 Braun, A., 2005. Carbon speciation in airborne particulate matter with C (1s)
599 NEXAFS spectroscopy. *J. Environ. Monit.* 7 (11), 1059–1065.

600 Braun, A., Huggins, F. E., Kelly, K. E., Mun, B. S., Ehrlich, S. N., Huffman,
601 G. P., 2006a. Impact of ferrocene on the structure of diesel exhaust soot as
602 probed with wide-angle X-ray scattering and C(1s) NEXAFS spectroscopy.
603 *Carbon* 44 (14), 2904–2911.

604 Braun, A., Huggins, F. E., Shah, N., Chen, Y., Wirick, S., Mun, S. B., Jacob-
605 sen, C., Huffman, G. P., 2005a. Advantages of soft X-ray absorption over
606 TEM-EELS for solid carbon studies - a comparative study on diesel soot
607 with EELS and nexafs. *Carbon* 43 (1), 117–124.

608 Braun, A., Mun, B. S., Huggins, F. E., Huffman, G. P., 2007. Carbon specia-
609 tion of diesel exhaust and urban particulate matter NIST standard reference
610 materials with C(1s) NEXAFS spectroscopy. *Environ. Sci. Technol.* 41 (1),
611 173–178.

612 Braun, A., Shah, N., Huggins, F. E., Huffman, G. P., Wirick, S., Jacobsen,
613 C., Kelly, K., Sarofim, A. F., 2004. A study of diesel PM with X-ray mi-
614 crospectroscopy. *Fuel* 83 (7-8), 997–1000.

615 Braun, A., Shah, N., Huggins, F. E., Kelly, K. E., Sarofim, A., Jacobsen, C.,
616 Wirick, S., Francis, H., Ilavsky, J., Thomas, G. E., Huffman, G. P., 2005b.
617 X-ray scattering and spectroscopy studies on diesel soot from oxygenated
618 fuel under various engine load conditions. *Carbon* 43 (12), 2588–2599.

619 Braun, A., Wirick, A., Kubatova, A., Mun, B. S., Huggins, F. E., 2006b.
620 Photochemically induced decarboxylation in diesel soot extracts. *Atmos.*
621 *Environ.* 40 (30), 5837–5844.

622 di Stasio, S., Braun, A., 2006. Comparative NEXAFS study on soot obtained
623 from an ethylene/air flame, a diesel engine, and graphite. *Energy Fuels*
624 20 (1), 187–194.

625 Draxler, R. R., Rolph, G. D., 2003. Hysplit (hybrid single-particle la-
626 grangian integrated trajectory). Model access via NOAA ARL READY
627 Website (<http://www.arl.noaa.gov/ready/hysplit4.html>). NOAA Air Re-
628 sources Laboratory, Silver Spring, MD.

629 Fine, P. M., Chakrabarti, B., Krudysz, M., Schauer, J. J., Sioutas, C., 2004.
630 Diurnal variations of individual organic compound constituents of ultra-
631 fine and accumulation mode particulate matter in the Los Angeles basin.
632 *Environ. Sci. Technol.* 38 (5), 1296–1304.

633 Fraser, M. P., Cass, G. R., Simoneit, B. R. T., 2003. Air quality model eval-
634 uation data for organics. 6. C-3-C-24 organic acids. *Environ. Sci. Technol.*
635 37 (3), 446–453.

636 Fuzzi, S., Andreae, M. O., Huebert, B. J., Kulmala, M., Bond, T. C., Boy, M.,
637 Doherty, S. J., Guenther, A., Kanakidou, M., Kawamura, K., Kerminen,
638 V. M., Lohmann, U., Russell, L. M., Poschl, U., 2006. Critical assessment
639 of the current state of scientific knowledge, terminology, and research needs
640 concerning the role of organic aerosols in the atmosphere, climate, and global
641 change. *Atmos. Chem. Phys.* 6, 2017–2038.

642 Gebhart, K. A., Schichtel, B. A., Barna, M. G., 2005. Directional biases in
643 back trajectories caused by model and input data. *J. Air Waste Manage.*
644 *Assoc.* 55 (11), 1649–1662.

645 Gelencser, A., Hoffer, A., Krivacsy, Z., Kiss, G., Molnar, A., Meszaros, E.,
646 2002. On the possible origin of humic matter in fine continental aerosol. *J.*
647 *Geophys. Res.-Atmos.* 107 (D12).

648 Glasius, M., Lahaniati, M., Calogirou, A., Bella, D. D., Jensen, N. R., Hjorth,

649 J., Kotzias, D., Larsen, B. R., 2000. Carboxylic acids in secondary aerosols
650 from oxidation of cyclic monoterpenes by ozone. *Environ. Sci. Technol.*
651 34 (6), 1001–1010.

652 Graber, E. R., Rudich, Y., 2006. Atmospheric HULIS: How humic-like are
653 they? A comprehensive and critical review. *Atmos. Chem. Phys.* 6, 729–
654 753.

655 Gysel, M., Weingartner, E., Nyeki, S., Paulsen, D., Baltensperger, U., Galam-
656 bos, I., Kiss, G., 2004. Hygroscopic properties of water-soluble matter and
657 humic-like organics in atmospheric fine aerosol. *Atmos. Chem. Phys.* 4, 35–
658 50.

659 Hamilton, J. F., Webb, P. J., Lewis, A. C., Hopkins, J. R., Smith, S., Davy, P.,
660 2004. Partially oxidised organic components in urban aerosol using gcxgc-
661 tof/ms. *Atmos. Chem. Phys.* 4, 1279–1290.

662 Hand, J. L., Malm, W. C., Laskin, A., Day, D., Lee, T., Wang, C., Carrico, C.,
663 Carrillo, J., Cowin, J. P., Collett, J., Iedema, M. J., 2005. Optical, physical,
664 and chemical properties of tar balls observed during the Yosemite Aerosol
665 Characterization study. *J. Geophys. Res. - Atmos.* 110 (D21).

666 Hoffer, A., Gelencser, A., Guyon, P., Kiss, G., Schmid, O., Frank, G. P., Ar-
667 taxo, P., Andreae, M. O., 2006. Optical properties of humic-like substances
668 (HULIS) in biomass-burning aerosols. *Atmos. Chem. Phys.* 6, 3563–3570.

669 Hopkins, R. J., Tivanski, A. V., Marten, B. D., Gilles, M. K., 2007. Chemical
670 bonding and structure of black carbon reference materials and individual
671 carbonaceous atmospheric aerosols. *J. Aerosol Sci.* 38, 573–591.

672 Huebert, B. J., Bates, T., Russell, P. B., Shi, G. Y., Kim, Y. J., Kawamura, K.,
673 Carmichael, G., Nakajima, T., 2003. An overview of ACE-Asia: Strategies
674 for quantifying the relationships between Asian aerosols and their climatic
675 impacts. *J. Geophys. Res. - Atmos.* 108 (D23).

676 Huebert, B. J., Howell, S. G., Covert, D., Bertram, T., Clarke, A., Anderson,
677 J. R., Lafleur, B. G., Seebaugh, W. R., Wilson, J. C., Gesler, D., Blomquist,
678 B., Fox, J., 2004. Pelti: Measuring the passing efficiency of an airborne low
679 turbulence aerosol inlet. *Aerosol Sci. Tech.* 38 (8), 803–826.

680 Jacobson, M. Z., 2000. A physically-based treatment of elemental carbon op-
681 tics: Implications for global direct forcing of aerosols. *Geophys. Res. Lett.*
682 27 (2), 217–220.

683 Jang, M., McDow, S. R., 1997. Products of benz[a]anthracene photodegrada-
684 tion in the presence of known organic constituents of atmospheric aerosols.
685 *Environ. Sci. Technol.* 31 (4), 1046–1053.

686 Johnson, K. S., Zuberi, B., Molina, L. T., Molina, M. J., Iedema, M. J., Cowin,
687 J. P., Gaspar, D. J., Wang, C., Laskin, A., 2005. Processing of soot in an
688 urban environment: case study from the Mexico City Metropolitan area.
689 *Atmos. Chem. Phys.* 5, 3033–3043.

690 Kanakidou, M., Seinfeld, J. H., Pandis, S. N., Barnes, I., Dentener, F. J.,
691 Facchini, M. C., Dingenen, R. V., Ervens, B., Nenes, A., Nielsen, C. J.,
692 Swietlicki, E., Putaud, J. P., Balkanski, Y., Fuzzi, S., Horth, J., Moort-
693 gat, G. K., Winterhalter, R., Myhre, C. E. L., Tsigaridis, K., Vignati, E.,
694 Stephanou, E. G., Wilson, J., 2005. Organic aerosol and global climate mod-
695 elling: a review. *Atmos. Chem. Phys.* 5, 1053–1123.

696 Katrib, Y., Martin, S. T., Rudich, Y., Davidovits, P., Jayne, J. T., Worsnop,
697 D. R., 2005. Density changes of aerosol particles as a result of chemical
698 reaction. *Atmos. Chem. Phys.* 5, 275–291.

699 Kawamura, K., Kaplan, I. R., 1987. Motor exhaust emissions as a primary
700 source for dicarboxylic-acids in los-angeles ambient air. *Environ. Sci. Tech-*
701 *nol.* 21 (1), 105–110.

702 Kawamura, K., Yasui, O., 2005. Diurnal changes in the distribution of di-

703 carboxylic acids, ketocarboxylic acids and dicarbonyls in the urban Tokyo
704 atmosphere. *Atmos. Environ.* 39 (10), 1945–1960.

705 Kis, V. K., Posfai, M., Labar, J. L., 2006. Nanostructure of atmospheric soot
706 particles. *Atmos. Environ.* 40 (29), 5533–5542.

707 Kondo, Y., Miyazaki, Y., Takegawa, N., Miyakawa, T., Weber, R. J., Jimenez,
708 J. L., Zhang, Q., Worsnop, D. R., 2007. Oxygenated and water-soluble or-
709 ganic aerosols in Tokyo. *J. Geophys. Res. - Atmos.* 112 (D1).

710 Laskin, A., Cowin, J. P., Iedema, M. J., 2006. Analysis of individual environ-
711 mental particles using modern methods of electron microscopy and X-ray
712 microanalysis. *J. Electron Spectrosc.* 150 (2-3), 260–274.

713 Laskin, A., Wietsma, T. W., Krueger, B. J., Grassian, V. H., 2005. Hetero-
714 geneous chemistry of individual mineral dust particles with nitric acid: A
715 combined CCSEM/EDX, ESEM, and ICP-MS study. *J. Geophys. Res. -*
716 *Atmos.* 110 (D10).

717 Lehmann, J., Liang, B. Q., Solomon, D., Lerotic, M., Luizao, F., Kinyangi, J.,
718 Schafer, T., Wirick, S., Jacobsen, C., 2005. Near-edge X-ray absorption fine
719 structure (NEXAFS) spectroscopy for mapping nano-scale distribution of
720 organic carbon forms in soil: Application to black carbon particles. *Global*
721 *Biogeochem. Cy.* 19 (1).

722 Lim, H. J., Turpin, B. J., 2002. Origins of primary and secondary organic
723 aerosol in Atlanta: Results of time-resolved measurements during the At-
724 lanta supersite experiment. *Environ. Sci. Technol.* 36 (21), 4489–4496.

725 Lim, H. J., Turpin, B. J., Russell, L. M., Bates, T. S., 2003. Organic and
726 elemental carbon measurements during ACE-Asia suggest a longer atmo-
727 spheric lifetime for elemental carbon. *Environ. Sci. Tech.* 37 (14), 3055–3061.

728 Limbeck, A., Puxbaum, H., Otter, L., Scholes, M. C., 2001. Semivolatile be-
729 havior of dicarboxylic acids and other polar organic species at a rural back-

730 ground site (Nylsvley, rsa). *Atmos. Environ.* 35 (10), 1853–1862.

731 Liu, D. Y., Rutherford, D., Kinsey, M., Prather, K. A., 1997. Real-time moni-
732 toring of pyrotechnically derived aerosol particles in the troposphere. *Anal.*
733 *Chem.* 69 (10), 1808–1814.

734 Maria, S. F., Russell, L. M., Gilles, M. K., Myneni, S. C. B., 2004. Organic
735 aerosol growth mechanisms and their climate-forcing implications. *Science*
736 306 (5703), 1921–1924.

737 Maria, S. F., Russell, L. M., Turpin, B. J., Porcja, R. J., 2002. Ftir measure-
738 ments of functional groups and organic mass in aerosol samples over the
739 caribbean. *Atmos. Environ.* 36 (33), 5185–5196.

740 Maria, S. F., Russell, L. M., Turpin, B. J., Porcja, R. J., Campos, T. L., We-
741 ber, R. J., Huebert, B. J., 2003. Source signatures of carbon monoxide and
742 organic functional groups in Asian Pacific Regional Aerosol Characteriza-
743 tion Experiment (ACE-Asia) submicron aerosol types. *J. Geophys. Res. -*
744 *Atmos.* 108 (D23).

745 Michelsen, H. A., Tivanski, A., Gilles, M. K., van Poppel, L. H., Dansson,
746 M. A., Buseck, P. R., 2006. Particle formation from pulsed laser irradiation
747 of soot aggregates studied with smps, tem, and nexafs. *Appl. Optics* in press.

748 Mishchenko, M. I., Lacis, A. A., Carlson, B. E., Travis, L. D., 1995. Non-
749 sphericity of dust-like tropospheric aerosols - implications for aerosol
750 remote-sensing and climate modeling. *Geophys. Res. Lett.* 22 (9), 1077–
751 1080.

752 Mishchenko, M. I., Liu, L., Travis, L. D., Lacis, A. A., 2004. Scattering and
753 radiative properties of semi-external versus external mixtures of different
754 aerosol types. *J. Quant. Spectrosc. Radiat. Transf.* 88 (1-3), 139–147.

755 Mochida, M., Katrib, Y., Jayne, J. T., Worsnop, D. R., Martin, S. T., 2006.
756 The relative importance of competing pathways for the formation of high-

757 molecular-weight peroxides in the ozonolysis of organic aerosol particles.
758 *Atmos. Chem. Phys.* 6, 4851–4866.

759 Myhre, C. E. L., Nielsen, C. J., 2004. Optical properties in the UV and visible
760 spectral region of organic acids relevant to tropospheric aerosols. *Atmos.*
761 *Chem. Phys.* 4, 1759–1769.

762 Myneni, S. C. B., 2002. Soft X-ray spectroscopy and spectromicroscopy studies
763 of organic molecules in the environment. *Rev. Mineral. Geochem.* 49, 485–
764 579.

765 Obenholzer, J., Poelt, P., Schroettner, H., Delgado, H., 2003. Volcanic De-
766 gassing. Geological Society of London, Ch. Particles From the Plume of
767 Popocatepetl Volcano, Mexico - the FESEM/EDS Approach.

768 Petters, M. D., Prenni, A. J., Kreidenweis, S. M., DeMott, P. J., Mat-
769 sunaga, A., Lim, Y. B., Ziemann, P. J., 2006. Chemical aging and the
770 hydrophobic-to-hydrophilic conversion of carbonaceous aerosol. *Geophys.*
771 *Res. Lett.* 33 (24).

772 Phares, D. J., Rhoads, K. P., Johnston, M. V., Wexler, A. S., 2003. Size-
773 resolved ultrafine particle composition analysis - 2. houston. *J. Geophys.*
774 *Res. - Atmos.* 108 (D7).

775 Plaschke, M., Rothe, J., Denecke, M. A., Fanghanel, T., 2004. Soft X-ray
776 spectromicroscopy of humic acid europium(III) complexation by comparison
777 to model substances. *J. Electron Spectrosc. Relat. Phenom.* 135 (1), 53–62.

778 Posfai, M., Anderson, J. R., Buseck, P. R., Sievering, H., 1999. Soot and sulfate
779 aerosol particles in the remote marine troposphere. *J. Geophys. Res.-Atmos.*
780 104 (D17), 21685–21693.

781 Ray, J., McDow, S. R., 2005. Dicarboxylic acid concentration trends and sam-
782 pling artifacts. *Atmos. Environ.* 39 (40), 7906–7919.

783 Rhoads, K. P., Phares, D. J., Wexler, A. S., Johnston, M. V., 2003. Size-

784 resolved ultrafine particle composition analysis, 1. atlanta. *J. Geophys. Res.*
785 - *Atmos.* 108 (D7).

786 Rogge, W. F., Hildemann, L. M., Mazurek, M. A., Cass, G. R., Simoneit, B.
787 R. T., 1998. Sources of fine organic aerosol. 9. Pine, oak and synthetic log
788 combustion in residential fireplaces. *Environ. Sci. Technol.* 32 (1), 13–22.

789 Rolph, G. D., 2003. Real-time environmental applications and display system
790 (ready). Website (<http://www.arl.noaa.gov/ready/hysplit4.html>). NOAA
791 Air Resources Laboratory, Silver Spring, MD.

792 Rudolph, J., Stupak, J., 2002. Determination of aromatic acids and nitrophen-
793 nols in atmospheric aerosols by capillary electrophoresis. *J. Chromatogr.*
794 *Sci.* 40 (4), 207–213.

795 Russell, L. M., Maria, S. F., Myneni, S. C. B., 2002. Mapping organic coatings
796 on atmospheric particles. *Geophys. Res. Lett.* 29 (16).

797 Schumacher, M., Christl, I., Scheinost, A. C., Jacobsen, C., Kretzschmar, R.,
798 2005. Chemical heterogeneity of organic soil colloids investigated by scan-
799 ning transmission X-ray microscopy and C-1s NEXAFS microspectroscopy.
800 *Environ. Sci. Tech.* 39 (23), 9094–9100.

801 Seinfeld, J. H., Pandis, S. N., 2006. *Atmospheric Chemistry and Physics*, 2nd
802 Edition. John Wiley & Sons, New York.

803 Semeniuk, T. A., Wise, M. E., Martin, S. T., Russell, L. M., Buseck, P. R.,
804 2006. Hygroscopic behavior of aerosol particles from biomass fires using
805 environmental transmission electron microscopy in press.

806 Solomon, D., Lehmann, J., Kinyangi, J., Liang, B. Q., Schafer, T., 2005. Car-
807 bon K-edge NEXAFS and FTIR-ATR spectroscopic investigation of organic
808 carbon speciation in soils. *Soil Sci. Soc. Am. J.* 69 (1), 107–119.

809 Stevens, B., Lenschow, D. H., Vali, G., Gerber, H., Bandy, A., Blomquist,
810 B., Brenguier, J. L., Bretherton, C. S., Burnet, F., Campos, T., Chai, S.,

811 Faloon, I., Friesen, D., Haimov, S., Laursen, K., Lilly, D. K., Loehrer,
812 S. M., Malinowski, S. P., Morley, B., Petters, M. D., Rogers, D. C., Russell,
813 L., Savic-Jovac, V., Snider, J. R., Straub, D., Szumowski, M. J., Takagi, H.,
814 Thornton, D. C., Tschudi, M., Twohy, C., Wetzal, M., van Zanten, M. C.,
815 2003. Dynamics and chemistry of marine stratocumulus - dycoms-ii. *B. Am.*
816 *Meteorol. Soc.* 84 (5), 579–+.

817 Stöhr, J., 1992. *NEXAFS Spectroscopy*. Springer-Verlag, Berlin.

818 Tivanski, A. V., Hopkins, R. J., Tyliczszak, T., Gilles, M. K., 2007. Oxy-
819 genated interface on biomass burn tar balls determined by single particle
820 scanning transmission x-ray microscopy. *J. Phys. Chem. A* 111, 5448–5458.

821 Tolocka, M. P., Lake, D. A., Johnston, M. V., Wexler, A. S., 2005. Size-resolved
822 fine and ultrafine particle composition in Baltimore, maryland. *J. Geophys.*
823 *Res. - Atmos.* 110 (D7).

824 van Poppel, L. H., Friedrich, H., Spinsby, J., Chung, S. H., Seinfeld, J. H.,
825 Buseck, P. R., 2005. Electron tomography of nanoparticle clusters: Implica-
826 tions for atmospheric lifetimes and radiative forcing of soot. *Geophys. Res.*
827 *Lett.* 32 (24).

828 Varrica, D., Dongarra, G., Sabatino, G., Monna, F., 2003. Inorganic geochem-
829 istry of roadway dust from the metropolitan area of Palermo, italy. *Environ.*
830 *Geol.* 44 (2), 222–230.

831 Wang, H. B., Kawamura, K., Ho, K. F., Lee, S. C., 2006. Low molecular
832 weight dicarboxylic acids, ketoacids, and dicarbonyls in the fine particles
833 from a roadway tunnel: Possible secondary production from the precursors.
834 *Environ. Sci. Technol.* 40 (20), 6255–6260.

835 Warwick, T., Ade, H., Hitchcock, H., Padmore, H., Rightor, E., Tonner, B.,
836 1997. Soft x-ray spectromicroscopy development for materials science at
837 the advanced light source. *Journal of Electron Spectroscopy and Related*

838 Phenomena 84, 85–98(14).

839 Weckwerth, G., 2001. Verification of traffic emitted aerosol components in the
840 ambient air of Cologne (germany). *Atmos. Environ.* 35 (32), 5525–5536.

841 Yoon, T. H., Benzerara, K., Ahn, S., Luthy, R. G., Tyliczszak, T., Brown,
842 G. E., 2006. Nanometer-scale chemical heterogeneities of black carbon ma-
843 terials and their impacts on PCB sorption properties: Soft X-ray spectro-
844 microscopy study. *Environ. Sci. Technol.* 40 (19), 5923–5929.

845 Yu, J. Z., Cocker, D. R., Griffin, R. J., Flagan, R. C., Seinfeld, J. H., 1999. Gas-
846 phase ozone oxidation of monoterpenes: Gaseous and particulate products.
847 *J. Atmos. Chem.* 34 (2), 207–258.

848 Zhang, Q., Alfarra, M. R., Worsnop, D. R., Allan, J. D., Coe, H., Cana-
849 garatna, M. R., Jimenez, J. L., 2005a. Deconvolution and quantification of
850 hydrocarbon-like and oxygenated organic aerosols based on aerosol mass
851 spectrometry. *Environ. Sci. Tech.* 39 (13), 4938–4952.

852 Zhang, Q., Worsnop, D. R., Canagaratna, M. R., Jimenez, J. L., 2005b.
853 Hydrocarbon-like and oxygenated organic aerosols in Pittsburgh: insights
854 into sources and processes of organic aerosols. *Atmos. Chem. Phys.* 5, 3289–
855 3311.

Table 1
Summary of samples analyzed by STXM

Field Campaign	Study Period Location	Min. Alt. (m)	Max. Alt. (m)	Number of Particles
PELTI	Jul 2000 Caribbean (NCAR C-130)	30	2300	75
ACE-Asia	Apr 2001 Sea of Japan (NCAR C-130)	30	3650	185
DYCOMS II	Jul 2001 NE Pacific S. Cal. coast (NCAR C-130)	200	540	106
New Jersey	Aug 2003 Princeton, New Jersey (ground site)		85	48
MILAGRO (Urban)	Mar 2006 Mexico City (urban ground site)		2200	69
MILAGRO (Aircraft)	Mar 2006 Mexico mainland/ Yucatan peninsula (NCAR C-130)	2090	4340	95
INTEX-B	May 2006 U.S. West coast (NCAR C-130)	890	1920	17
Total				595

Campaign	Spectra Type													
	(a)	(b)	(c)	(d)	(e)	(f)	(g)	(h)	(i)	(j)	(k)	(l)	(m)	(n)
PELTI	14	0	0	4	5	12	0	0	14	4	23	4	0	0
DYCOMS II	41	0	25	4	2	0	0	0	14	5	16	18	10	0
ACE-Asia	46	0	0	0	0	0	0	0	2	4	17	2	0	0
New Jersey	3	0	0	3	15	0	9	0	2	2	4	10	0	0
MILAGRO (Urban)	22	0	0	4	3	0	0	9	15	10	2	5	3	8
MILAGRO (Aircraft)	9	21	0	18	8	0	2	1	6	6	7	23	1	1
INTEX-B	6	0	1	2	2	0	0	0	6	0	0	2	0	1
Total	141	21	26	35	35	12	11	10	59	31	69	64	14	10

Table 2
%sp² Hybridization

Metaclass	Type	Mean (%)	Standard deviation (%)
Strongly aromatic	b	48	5
	c	40	12
	d	72	15
	e	56	10
	g	29	8
	h	39	18
Multiple transition	m	28	18
	i	18	15
	j	30	20

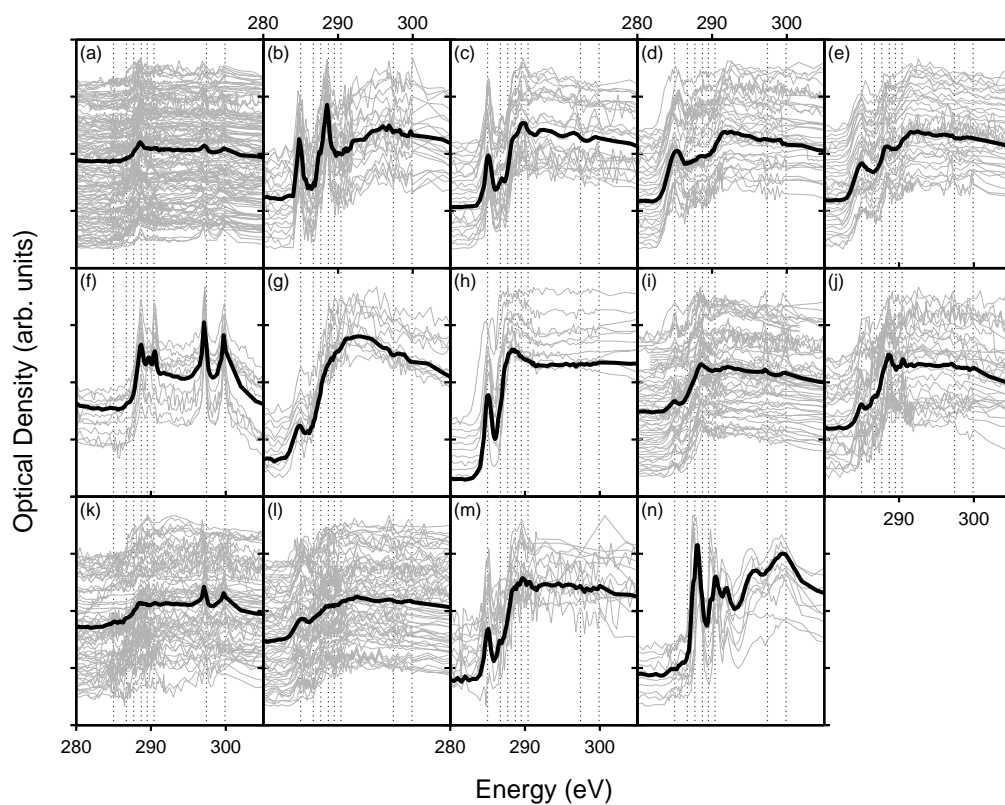


Fig. 1. Fourteen classifications of spectra. Gray lines are scaled individual spectra; dark lines are averages of all spectra. Individual spectra include arbitrary shifts on the vertical axis to display them separately. Vertical lines at 285, 286.7, 287.7, 288.7, and 290.4 eV represent $R(C=C)R'$, $R(C=O)R$, $R(CH_n)R'$, $R(C=O)OH$, and CO_3^{2-} transitions, respectively.

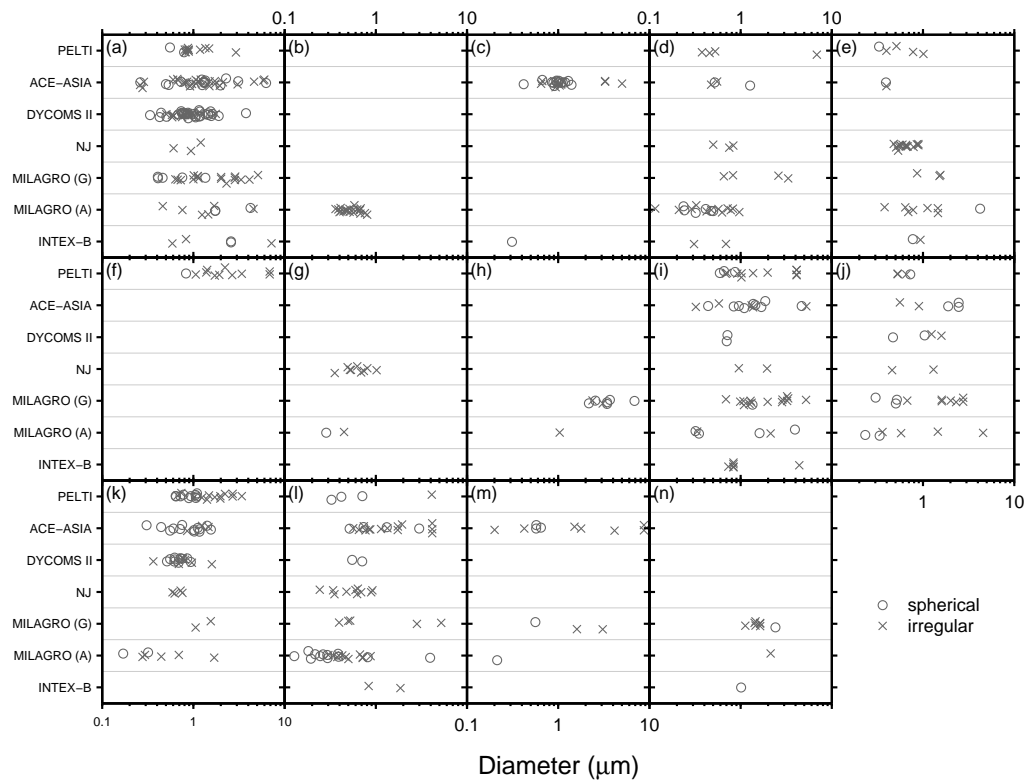


Fig. 2. Size and shape classification of particles by spectra type; each panel corresponds to the spectra shown in respective panels of Figure 1. Circles indicate spherical particles, and crosses indicate irregular particles.

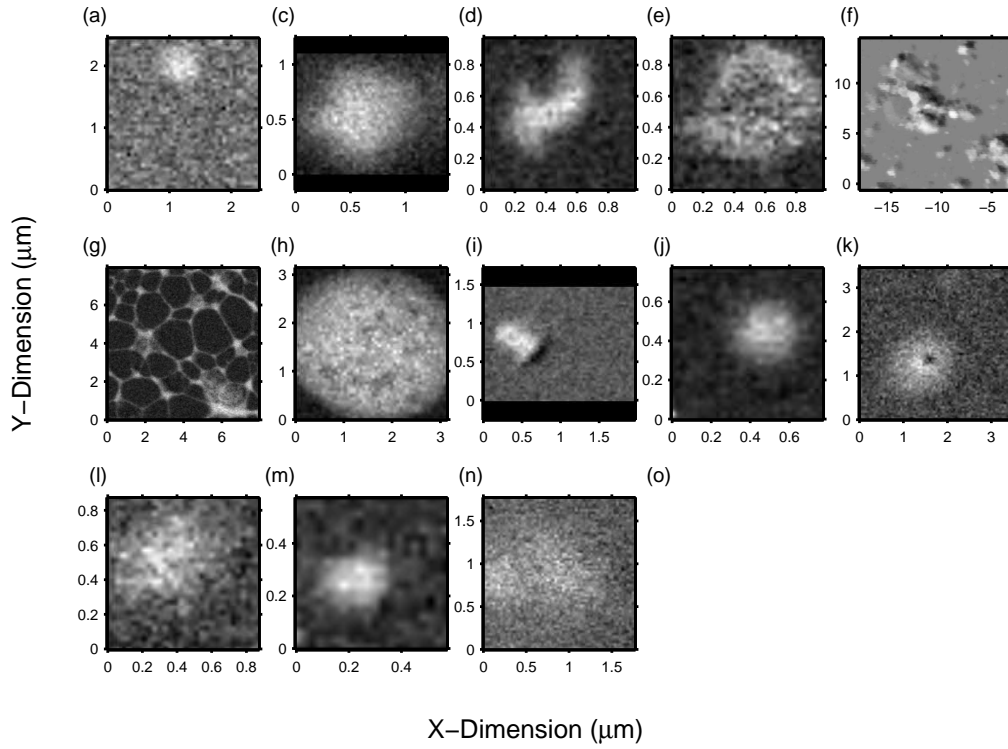


Fig. 3. Example images for each category; each panel corresponds to respective panels in Figure 1. Particles are from (a) ACE-ASIA, (b) MILAGRO (A), (c) ACE-ASIA, (d) MILAGRO (A), (e) MILAGRO (U), (f) PELTI, (g) Princeton, (h) MILAGRO (U), (i) ACE-ASIA, (j) MILAGRO (A), (k) ACE-ASIA, (l) MILAGRO (A), (m) MILAGRO (A), (n) MILAGRO (U).

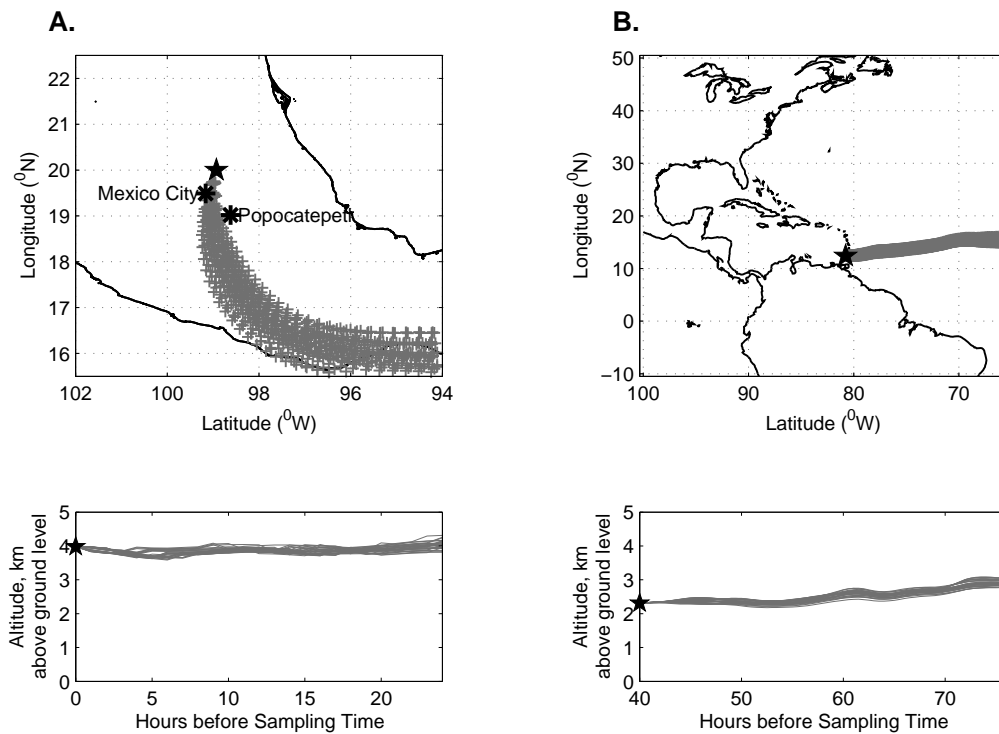


Fig. 4. Backtrajectories obtained from NOAA HYSPLIT simulations for particle types b (Panel A) and f (Panel B). Star symbol indicates locations from which backtrajectories were calculated. Initial conditions, Panel A: 3/18/06 21:00 GMT, 20.00N, 98.93W, 3980 m above MSL, 24-hour duration; Panel B: 2000-07-21 15:00 GMT, 23.39N, 61.55W, 2470 m above MSL, 72-hour duration.

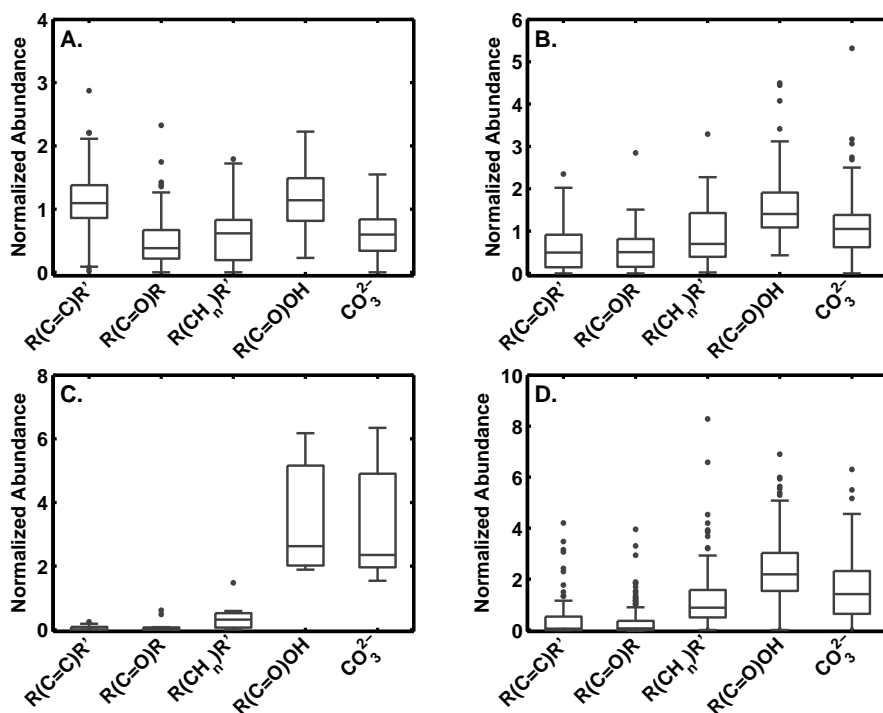


Fig. 5. Peak areas normalized by total carbon content for four meta-classes: Panel A, strongly aromatic; Panel B, multiple-transition; Panel C, carbonate and carboxylic-carbonyl; and Panel D, carboxylic-carbonyl dominated aerosols. Boxes encompass the 25th to 75th percentile of the data, lines within boxes represent the median value, and whiskers span 1.5 times the interquartile range. Circles represent data points that lie outside of this range.

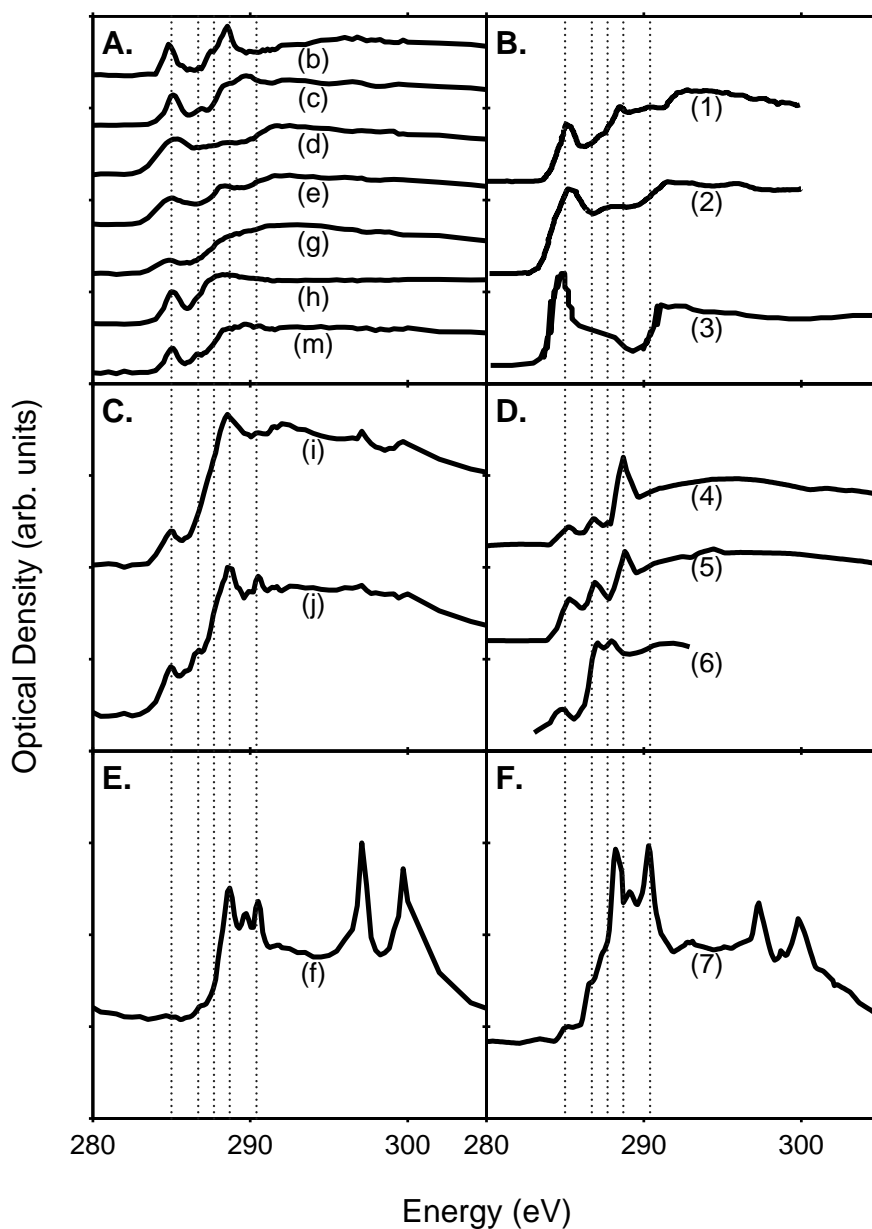


Fig. 6. NEXAFS spectra of reference material. Panels A, C, and E are spectra shown in 1. Panel A, average spectra of strongly aromatic aerosols. Panel B, combustion-derived aerosol: (1) black-carbon-like spectra of marine particulate organic matter from factor analysis (Brandes et al., 2004), (2) diesel soot (Braun, 2005), (3) graphitic carbon (di Stasio and Braun, 2006). Panel C, average spectra of multiple-transition aerosols. Panel D, (4) fulvic acid (Ade and Urquhart, 2002), (5) humic acid (Ade and Urquhart, 2002), (6) wood-smoke particles collected on a chimney (Braun, 2005). Panel E, average spectra of carbonate and carboxylic-carbonyl aerosol (type f) particles collected over the Caribbean Ocean during during PELTI campaign. Panel F, (7) pine Ultisol soil (Ade and Urquhart, 2002). Vertical lines at 285, 286.7, 287.7, 288.7, and 290.4 eV represent $R(C=C)R'$, $R(C=O)R$, $R(CH_n)R'$, $R(C=O)OH$, and CO_3^{2-} transitions, respectively.